

Mic-Mac model based on the Wigner-Kirkwood method

A. Bhagwat¹, M. Centelles^{2,3}, X. Viñas^{2,3,4}, R. Wyss⁵

¹ UM-DAE Centre for Excellence in Basic Sciences, Mumbai 400 098, India

² Departament de Física Quàntica i Astrofísica (FQA), Universitat de Barcelona (UB), Martí i Franquès 1, E-08028 Barcelona, Spain

³ Institut de Ciències del Cosmos (ICCUB), Universitat de Barcelona (UB), Martí i Franquès 1, E-08028 Barcelona, Spain

⁴ Institut Menorquí d'Estudis, Camí des Castell 28, E-07702 Maó, Spain

⁵ KTH (Royal Institute of Technology), Alba Nova University Center, Department of Nuclear Physics, S-10691 Stockholm, Sweden

Received: date / Revised version: date

Abstract. About a decade ago we proposed a new Microscopic-Macroscopic (Mic-Mac) model where the semiclassical Wigner-Kirkwood expansion of the energy up to fourth-order in \hbar is used to compute the shell corrections in a deformed Woods-Saxon potential instead of the usual Strutinsky averaging scheme [1, 2]. For a set of 551 even-even nuclei computed with this new model, we found a *rms* deviation of 610 keV from the experimental masses, similar to the value obtained using the well-known Finite Range Droplet Model and the Lublin-Strasbourg Drop Model for the same set of nuclei. In a next step, we compute the ground-state properties of these 551 nuclei with the same method but using the mean-field provided by the Gogny forces within an Extended Thomas-Fermi approximation. We find that this Mic-Mac model using the Gogny D1S (D1M) force gives a fairly good description of the ground-state energies with a *rms* deviation of 834 keV (819 keV). This implies that Mic-Mac models based on effective two-body forces, for example Gogny D1S and D1M interactions, perform practically as well as the most efficient Mic-Mac models regarding ground-state properties.

PACS. XX.XX.XX No PACS code given

1 Introduction

Masses constitute a fundamental observable of atomic nuclei. However, theoretical determination of nuclear masses with high accuracy is still an open problem in Nuclear Physics. The comparison between theory and experiment provides a benchmark on the quality of nuclear models. The recent development in Nuclear Physics with the advent of radioactive ion beams, has opened up the nuclear chart to nuclei far from the line of stability. The current efforts at the newly built and/or soon to be constructed experimental nuclear facilities will further expand our knowledge of exotic nuclei far from stability (see, for example, [3]). This will provide additional constraints on the quality of nuclear models and deepen our understanding of the effective nuclear force. The measurement of nuclei far from stability sets new constraints on the astrophysical processes that are responsible for the creation of the elements. Also here, the nuclear mass is a key ingredient to calculations determining the details of, e.g., the r-process.

There are in principle two classes of models used to calculate nuclear masses: The most common model, of the so-called Microscopic-Macroscopic (Mic-Mac) type, combines quantal corrections obtained from a phenomenological potential with the total energy of the liquid drop,

fitted to measured masses. The quantal corrections can be obtained by means of the Strutinsky method, which is a well defined mathematical procedure for dealing with the smoothing of shell effects in finite nuclei. As shown in this paper, our group developed an alternative method for the calculation of the shell corrections based on the Wigner-Kirkwood (WK) expansion of the density matrix. The other class of models are fully microscopic employing effective interactions like Skyrme [4–9] and Gogny [10–13] forces or based on effective covariant Lagrangians, like the relativistic mean field models (see, for example, [14]).

In our work we further developed methods to merge the two different classes of models, by deriving the potential from the microscopic Gogny interaction. The method is not restricted to any particular force and will actually shed insight into possible deficiencies present in the force used for our calculations. We employ the standard shell correction method where the energy shell correction δE is that of the mean-field leading-order component.

The paper is organized as follows. In section two, we review the common methods available for computing the shell corrections. In section three, we present the Woods-Saxon model used for our calculations jointly with the WK method to obtain the quantal corrections to the liq-

uid drop model. Note that the Woods-Saxon potential that is used for our mass calculations has been derived to fit single-particle energies in magical nuclei and has been widely employed to describe the ground state of nuclei as well as the highest angular momentum and super-deformation. It accounts well for nuclear charge radii and has not been fitted in particular to account for masses.

In section four, we analyze the predictions for nuclear masses from the Mic-Mac model based on the WK method in comparison with the results from other Mic-Mac models well known in the literature. In section five, we review our work made with the Gogny force in deriving a microscopic nuclear potential and the application of the WK-Gogny Mic-Mac method for mass calculations. In section six, we perform further investigations of the mass predictions from the WK-based Mic-Mac model. Finally, in the last section, we present a summary and our conclusions.

In this review paper, we recall and honor key aspects of our collaboration with Peter Schuck, who made immense contributions to the entire field of nuclear physics. With his unique knowledge on semi-classical methods, he provided deep insight, inspiration and guidance to our work.

2 Shell correction methods

The theoretical foundation of the splitting of the nuclear masses into a part that varies smoothly with the atomic and mass numbers and another part that is strongly oscillating lies on the so-called Strutinsky energy theorem [15], which divides the total energy as $E = \bar{E} + \delta E$. The larger part, \bar{E} , varies smoothly with the nucleon number and can be associated to the liquid drop energy. The smaller part, δE , is oscillating and corresponds to the shell energy that can be estimated within the shell model in an external potential. The calculation of δE can be performed from the exact energy E but replacing in the density matrix the quantal occupation numbers by the smooth ones obtained through the Strutinsky averaging method.

The smoothing of the total energy E can also be obtained from the Wigner-Kirkwood (WK) expansion of the density matrix [16]. In this approach, the single-particle and the kinetic energy densities are expressed by means of functionals of the one-body single-particle mean field V . The WK expansion of the particle and kinetic energy densities diverges at the classical turning point. These quantities should be considered as distributions rather than as functions [16,17] in the sense that only the integrated quantities, i.e. number of particles and kinetic energy, have physical meaning. Another important property of the WK expansion in powers of \hbar is its variational content. For a set of non-interacting fermions in an external potential well, the variational solution for the particle density that minimizes the semiclassical WK energy at each order of the \hbar expansion, is the particle density at the same order in \hbar [18,19]. In this approach, the shell correction is simply given by the difference between the quantal and WK total energies.

A slightly different method, also based on the WK expansion, is the Extended Thomas-Fermi (ETF) approach.

It allows one to express, by elimination of the single-particle potential, the kinetic energy density as a functional of the particle density ρ and its gradients [20]. The combination of the ETF kinetic energy density with a potential energy density functional, as the one provided by Skyrme forces, leads to the Density Functional Theory (DFT). The ground-state particle density is obtained by the variational principle and the theoretical justification is provided by the Hohenberg-Kohn theorem [21]. In the DFT formalism, the shell corrections can be estimated by the so-called Strutinsky integral method [22]. In this method, the shell correction is obtained from the difference between the sum of the lowest occupied single-particle levels and the corresponding semiclassical counterpart of the single-particle mean field potential computed with the density solution of the variational problem (see an explicit example of this method for a functional based on the Gogny force in [23]). The WK and ETF methods exhibit small but significant differences. On the one hand, the turning point of the WK expansion is pushed to infinity, and, on the other hand, the variational content of the WK expansion is not preserved, as far as ETF does not properly sort out the different powers of \hbar and partially adds terms to all orders in \hbar [18,19]. The small differences between the WK and ETF methods can be appreciated in Figures 1 and 2 of [19], where the energy per particle calculated with the WK and ETF methods is displayed for a set of fermions in harmonic oscillator and Woods-Saxon external potentials.

The connection between the Strutinsky and WK level densities has been recently discussed in Ref.[24]. This paper presents an analytical link in the asymptotic limit between the level density obtained through the Strutinsky method and in the semiclassical (WK) approximation. The Strutinsky averaging is established rigorously through a least-squares approximation of the level density, as suggested earlier in Ref.[25]. The Strutinsky average depends on two open parameters, namely, the smoothing parameter γ and the degree M of the fitting polynomial. At difference with the semiclassical approach, the Strutinsky average contains an intrinsic noise (remainder), which is proportional to $(\gamma/\lambda)^M$ with λ the chemical potential. For realistic potentials in the asymptotic limit and far from the drip lines, i.e. $\lambda \ll 0$, this remainder is small, specially for high values of M , and therefore the Strutinsky method averages well level densities and energies. This can be seen in, e.g., Figures 1 and 2 of [19] where there is an excellent agreement between Strutinsky and WK calculations. However, for realistic potentials near the drip point (weakly bound nuclei) where $\lambda \rightarrow 0$, due to the singularity of the semiclassical level density at the top of the well, the Strutinsky averaging strongly depends on the value of γ and can get compromised in this region (see in this respect Fig.6 of Ref.[24]).

3 Theoretical framework

3.1 The Wigner-Kirkwood energy

The key quantity for describing a system of N interacting fermions at zero temperature in an external potential well is the partition function, given by

$$Z(\beta) = \text{Tr} \left(\exp(-\beta \hat{H}) \right), \quad (1)$$

where the Hamiltonian of the system is expressed by

$$\hat{H} = \frac{-\hbar^2}{2m} \nabla^2 + V(\mathbf{r}) + \hat{V}_{LS}(\mathbf{r}). \quad (2)$$

In Eq.(2) $V(\mathbf{r})$ is the central potential and $\hat{V}_{LS}(\mathbf{r})$ the spin-orbit potential that, in general, can be written as:

$$\hat{V}_{LS} = \frac{\nu \kappa \hbar^2}{2m} (\nabla f \times \nabla) \cdot \hat{\sigma}, \quad (3)$$

where $\hat{\sigma}$ is the unit Pauli matrix, κ is the strength of the spin-orbit interaction, and f is the spin-orbit form factor.

The semiclassical WK partition function is obtained by performing the expansion of Eq.(1) in powers of \hbar [16, 20, 26–31]. The lowest order of this expansion corresponds to the well-known Thomas-Fermi (TF) approach and the additional powers of \hbar yield systematic corrections to the TF energy and particle numbers. The semiclassical WK partition function up to the fourth order in \hbar can be schematically expressed as:

$$Z_{WK}^{(4)}(\beta) = Z^{(4)}(\beta) + Z_{SO}^{(4)}(\beta). \quad (4)$$

where, $Z^{(4)}(\beta)$ ($Z_{SO}^{(4)}(\beta)$) is the WK partition function for the central potential (spin - orbit part). Explicit expressions for these partition functions including the spin-orbit contribution to the nuclear potential can be found in Refs.[1, 28].

Following Ref.[28], we write the WK energy as

$$E_{WK} = \lambda N - (E_{\hbar^0}^{CN} + E_{\hbar^2}^{CN} + E_{\hbar^4}^{CN}) - (E_{\hbar^2}^{SO} + E_{\hbar^4}^{SO}) \quad (5)$$

where $E_{\hbar^k}^{CN}$ and $E_{\hbar^k}^{SO}$ denote the contribution to the energy of the order \hbar^k arising from Laplace inversion of the central and spin-orbit parts of the partition function (4), respectively. Explicit expressions of each contribution to the WK energy in Eq.(5) are reported in Ref.[2].

3.2 The single-particle potential

In our model the nuclear mean field is taken of the Woods-Saxon (WS) type:

$$V(r) = \frac{V_0}{1 + \exp[l(\mathbf{r})/a]}, \quad (6)$$

where V_0 is the strength of the potential, a the diffuseness and $l(\mathbf{r})$ is the distance function. As in our previous works

[1, 2, 32], we follow the treatment of the distance function for a deformed WS potential as defined by Ref.[33], requiring that the skin thickness remains constant along the nuclear surface. For our calculation of nuclear masses, we consider three degrees of freedom, namely, β_2 , β_4 and γ , which are related with the parameters $\alpha_{\lambda, \mu}$ (see [1, 33, 34] for the explicit relations and other details).

The full single-particle potential needed to obtain the energy consists of the central, spin-orbit and Coulomb contributions. The central part is given by (6) and the spin-orbit potential by Eq.(3) with a form factor given by

$$f(r) = \frac{1}{1 + \exp[l(\mathbf{r})/a]}. \quad (7)$$

The parameters that define the central and spin - orbit parts of the single - particle potential are reported in Ref.[1]. The corresponding strengths and the half-density radius (the same for the central and spin-orbit contributions) have isospin dependence. The diffuseness parameter is assumed to be the same for neutron and protons in both, central and spin-orbit, parts. This potential yields a reasonably good description of charge radii (both magnitude and isospin dependence) [35] as well as of the moments of inertia for a wide range of nuclei. It is also quite successful in reproducing energies of single-particle and collective states [36]. The Coulomb potential is obtained by folding the proton density distribution with the Coulomb interaction. For simplicity the proton density is assumed to be of the WS type with the same parameters of the nuclear potential for protons. The reason of using a folded potential is that the WK expansion is not valid for potentials with sharp surfaces, which invalidates the hard-sphere approach for the Coulomb potential. The mass model constructed using the Woods - Saxon potential and the Coulomb potential thus obtained is labeled ‘StkI’ in this work, whereas the Woods - Saxon parameters are labeled ‘Stockholm-I’ parameters.

One of the apparent drawbacks of the StkI model is that there is a slight inconsistency in it. The Woods - Saxon parameters (mean field as well as spin - orbit) have been obtained for the hard-sphere approximation for Coulomb potential, whereas the mass calculation has been done by assuming a potential that has a surface with finite diffusivity. This leads to a bit less repulsive Coulomb potential as discussed in Ref. [1], thereby shifting the proton single-particle states slightly. One of the ways of removing this inconsistency is to renormalise the Woods - Saxon potential parameters in this case, through a re-fit to the measured single-particle states. The StkI model thus requires the Woods - Saxon parameters to be consistent with the new Coulomb potential.

In the following we treat the charge density assuming a Fermi function form with the parameters fitted to measured charge radii [35] of 132 spherical nuclei. The half-density radius was assumed to be of the form:

$$R_{1/2} = r_0 (1 + r_1 I + r_2 I^2) A^{1/3} \quad (8)$$

where, $I = (N - Z)/A$. The three parameters, r_0 , r_1 and r_2 along with the diffusivity parameter a were considered to

be free parameters of the model, and were determined using the standard Levenberg-Marquardt optimisation procedure. Their explicit values are: $r_0 = 1.231$, $r_1 = -0.332$, $r_3 = 0.461$ and $a = 0.320$. The value of the *rms* deviation turned out to be merely 0.017 fm, indicating that the fit is indeed reliable. It implies that our folded charge density is not consistent with the parameters of the Woods Saxon potential that is used for the nuclear mean field. Still, we expect this inconsistency to be of minor importance.

The Stockholm-I parameters were then re-fitted to reproduce some of the measured single-particle states of selected spherical nuclei. It turned out that it is sufficient to adjust only the strengths of the mean field. Specifically, it was assumed that the strengths are parameterised by

$$V^{(n)} = V_0^{(n)} (1 - \kappa_n |I|) \quad (9)$$

$$V^{(p)} = V_0^{(p)} (1 + \kappa_p |I|). \quad (10)$$

Using Powell's algorithm for χ^2 minimisation, the parameters were determined and their explicit values turn out to be: $V_0^{(n)} = 53.084$ MeV, $V_0^{(p)} = 53.095$ MeV, $\kappa_n = 0.779$ and $\kappa_p = 0.912$. The single-particle states turn out to be equally well - described in this fit as compared to the one used Stockholm - I potential. The mass model constructed using this modified single-particle potential will be labeled 'StkII' and the Woods - Saxon parameters will be labeled 'Stockholm-II' parameters in this work.

3.3 The microscopic contribution to the energy

The total shell correction of a nucleus is the sum of the neutron and proton shell corrections. For each kind of nucleons, the shell correction is given by the difference between the quantum mechanical and the averaged energies. In our approach the shell correction is obtained by subtracting the semiclassical WK energy from the quantal energy, which is the sum of the eigenvalues obtained by solving the Schrödinger equation for a set of nucleons moving in the corresponding single-particle potential well.

It may be interesting to compare the shell correction obtained using the WK approach for the average energy with the results provided by the Strutinsky average. To this end we have performed WK and Strutinsky calculations of the shell energy along the Ni and Sn isotopic chains with the StkI and StkII potentials discussed in the previous subsection (spherical symmetry has been assumed in this case) and the corresponding results are displayed in Fig.1.

We can see that both, the WK and Strutinsky results, show similar trends. As expected, we can see, on the one hand, that WK and Strutinsky shell corrections obtained using the StkI and StkII potentials are practically identical. On the other hand, we can also see that the WK and Strutinsky results computed with these two potentials for both considered isotopic chains show similar trends. As expected, both isotopic chains show prominent minima for neutron numbers corresponding to double shell closures: $N=28, 34, 40$ and 50 (Ni isotopes) and $N=50$ and 82 (Sn

isotopic chain). Along these isotopic chains, in particular at mid-shell, the WK shell corrections are somewhat stronger than the ones obtained in the Strutinsky calculation, with the former shifted with respect to the latter by an amount of 1-2 MeV. In spite that for nuclei far from the drip lines the Strutinsky and WK methods predict quite close shell corrections, larger differences may exist between the corrections computed with the two methods in nuclei at the drip lines, as discussed in detail in Ref. [24] (see in particular Figure 6 of this reference).

The pairing correlations, important for describing open shell nuclei, have also been included in the microscopic part of the energy. In our model, pairing is treated using the Lipkin-Nogami scheme [37–39], which allows to overcome the difficulties associated to the BCS scheme (see [1] for more details).

3.4 The macroscopic contribution to the energy

Following [2], the LDM part of the binding energy is written as

$$E_{LDM} = a_v \left[1 + \frac{4k_v}{A^2} T_z (T_z + 1) \right] A + a_s \left[1 + \frac{4k_s}{A^2} T_z (T_z + 1) \right] A^{2/3}$$

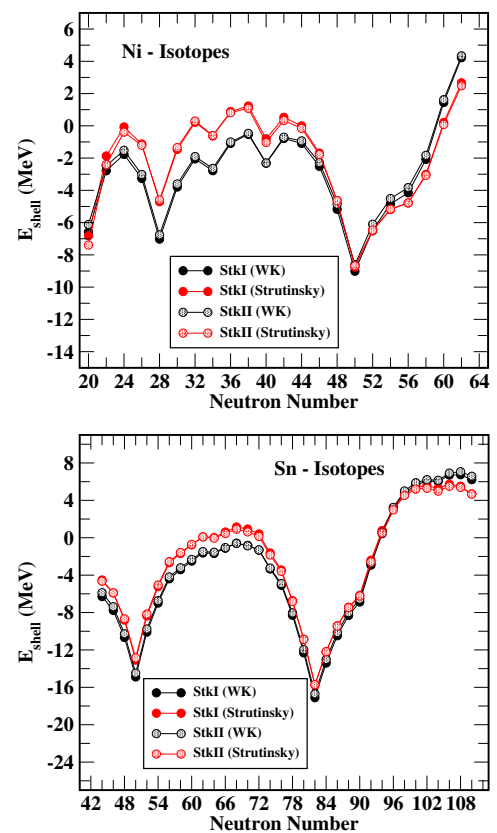


Fig. 1. Comparison between Wigner-Kirkwood and Strutinsky shell corrections along the Ni and Sn isotopic chains (see text for more details).

$$\begin{aligned}
& + a_{cur} \left[1 + \frac{4k_{cur}}{A^2} T_z (T_z + 1) \right] A^{1/3} \\
& + \frac{3Z^2 e^2}{5r_0 A^{1/3}} + \frac{C_4 Z^2}{A} + E_W, \quad (11)
\end{aligned}$$

where the different terms represent the volume energy, the surface energy, the curvature energy, the Coulomb energy, the correction to Coulomb energy due to surface diffuseness of the charge distribution and the Wigner energy, respectively. The coefficients a_v , a_s , a_{cur} , k_v , k_s , k_{cur} , r_0 and C_4 are free parameters; T_z is the third component of isospin, and e is the electron charge. For the Wigner energy, E_W , we adopt the following ansatz

$$E_W = w_1 \exp \left\{ -w_2 \left| \frac{N - Z}{A} \right| \right\} \Theta(Z - 20) \Theta(A - 40), \quad (12)$$

where, w_1 and w_2 are free parameters. The cut offs on charge and mass numbers have been introduced since it is expected that the Wigner term will make significant contributions for nuclei with low masses. The deformation effects have explicitly been included in the Coulomb, surface and curvature energies in Eq.(11), details of which can be found in [2].

3.5 The total energy in the Wigner-Kirkwood Microscopic-Macroscopic model

The total energy in our model of a nucleus containing N neutrons and Z protons and deformation parameters β_2 , β_4 and γ is given by

$$\begin{aligned}
E(N, Z, \beta_2, \beta_4, \gamma) & = E_{LDM}(N, Z, \beta_2, \beta_4, \gamma) \\
& + \eta \delta E(N, Z, \beta_2, \beta_4, \gamma), \quad (13)
\end{aligned}$$

where δE represents the microscopic part of the binding energy (shell correction plus pairing energy). The microscopic part has been multiplied by a factor $\eta=0.85$ to account for the fact that the Coulomb potential used in the present work is less repulsive near $r = 0$ than the Coulomb potential calculated in ‘sharp surface’ approximation used in the fit of the proton mean field (see [1] for more details).

The free parameters of the liquid drop formula (11), namely a_v , a_s , a_{cur} , k_v , k_s , r_0 , C_4 , w_1 and w_2 are determined by minimizing the χ^2 value respect the experimental energies [50] of 561 even-even spherical nuclei with $Z \geq 8$ and $N \geq 8$ following the procedure explained in detail in Ref.[2].

It is important to note that the coefficient of the isospin dependent term in the curvature energy, k_{cur} , is very difficult to determine using experimental masses. In our fit, the resulting statistical error in this parameter turns out to be more than 50% of its value. Further, this term is found to weaken the strength of the isospin dependent term in the surface energy by a factor of 5. Therefore, the isospin dependence of the curvature term has been dropped in the present fit. The values of the LDM parameters of our model are given in Table 1. Large-scale Mic-Mac calcu-

Table 1. Values of the liquid drop parameters obtained through the χ^2 minimization for StkI and StkII models.

Quantity	StkI	StkII
a_v (MeV)	-15.435	-15.458
k_v	-1.875	-1.873
a_s (MeV)	16.673	16.855
k_s	-2.430	-2.408
a_{cur} (MeV)	3.161	2.790
r_0 (fm)	1.219	1.219
C_4 (MeV)	0.963	0.985
w_1 (MeV)	-2.763	-2.650
w_2	3.725	4.016
<i>rms dev.</i> (MeV)	0.610	0.613

lations, such as the tabulation of masses along the whole periodic table, demand fast computational codes. In this respect we have shown in [2] that the ratio between the fourth-order to second-order WK energies (see Eq.(5)) behaves in a very systematic manner and that this ratio can be parametrised accurately by a simple expression implying that the fourth-order corrections can be absorbed into the second-order contributions in a very simple way [2]. Using this absorption of the \hbar^4 contributions into the \hbar^2 ones, we practically recover the same parameters for the macroscopic part without deterioration of the quality achieved with the full WK calculation including explicitly the fourth-order contributions.

4 Mass predictions from the Wigner-Kirkwood microscopic-macroscopic model

In Figure 2 we show the nuclear mass chart computed with our Mic-Mac models built up with the phenomenological single-particle Woods-Saxon potentials Stockholm-I (StkI) [1] and Stockholm-II (StkII), discussed previously in this work, where the shell corrections are obtained using the WK expansion. In the same figure, the StkI and StkII results are compared with those of the Mic-Mac Finite-Range Droplet Model of Möller and Nix (MN) [40] and of the Lublin-Strasbourg Drop Model (LSD) [41], where the shell corrections were computed using the Strutinsky averaging method. The net *rms* deviation of the binding energies of 551 spherical and deformed even-even nuclei calculated with the Stockholm-WK models with respect to the experimental values are 609 keV (StkI) and 607 keV (StkII). The MN [40] and LSD [41] models yield, for the same set of nuclei, *rms* deviations of 657 keV and 630 keV, respectively. The differences between the calculated and experimental binding energies are displayed in Figure 2.

To get more insight about the ability of the WK model in describing binding energies along the periodic table, we report in Table 2 the partial *rms* deviation corresponding to different regions of the mass number compared with the values obtained using the different models analyzed in

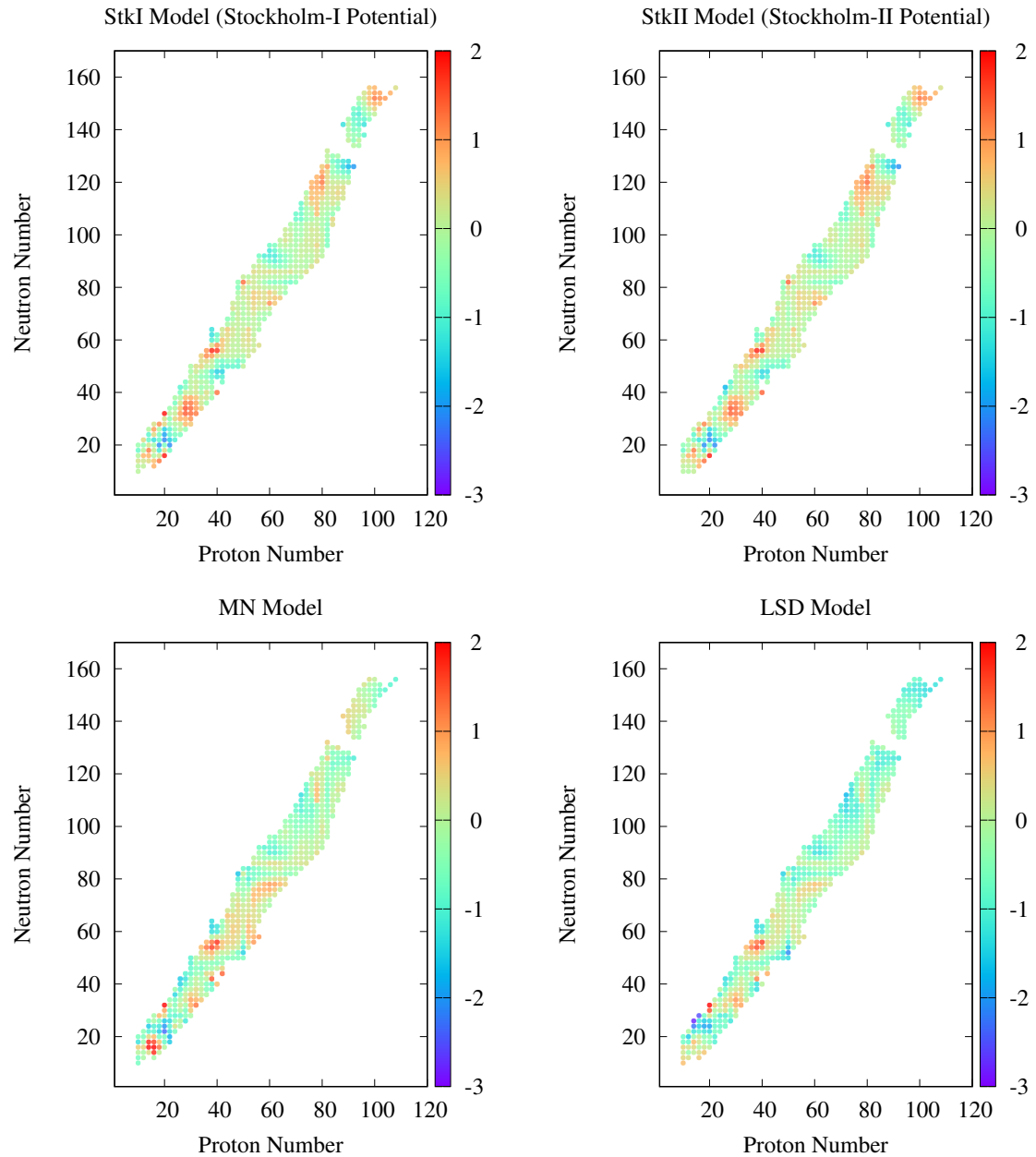


Fig. 2. Nuclear chart of theoretical minus experimental energies along the periodic table computed with the Mic-Mac based on the Wigner-Kirkwood method using the Stockholm-I (upper left) and Stockholm-II (upper right) phenomenological mean-field potentials discussed in this paper. The Mic-Mac predictions of the Finite-Range Droplet Model [40] and of the Lublin-Strasbourg-Drop parametrisation [41], which compute the shell corrections using the Strutinsky averaging method, are displayed in the lower left and lower right panels.

this work. It can be seen that all the considered Mic-Mac models do not describe very accurately the binding energies of nuclei with mass number smaller than 100. For the 160 nuclei considered in this region the *rms* deviations are 808, 795, 895 and 940 keV when the binding energies are calculated with the StkI, StkII, LSD and MN models, respectively. In the region of mass numbers between 100 and 200, where we have considered 301 nuclei, the calculated binding energies are in much better agreement with the experimental values, being the *rms* deviation 422, 424, 502

and 503 keV when the calculation is performed using the StkI, StkII, LSD and MN models, respectively. Globally for the 461 nuclei with mass numbers smaller than 200, the predictions of the Stockholm model are slightly better than the ones obtained using the LSD and MN models. In this case the *rms* deviations of the StkI and StkII calculations are 584 and 579 keV, while they are 673 and 695 keV if the energies are computed with the LSD and MN models. However, the Stockholm model is slightly less competitive for nuclei with mass number above 200. For

Table 2. Values of the rms deviation with respect to experiment of the binding energies (in keV) corresponding to different regions of the mass number (A) obtained using the WK, LSD [41] and MN [40] Mic-Mac models.

Model	Mass Regions (Number of Nuclides)				Net <i>rms</i> dev. (551 Nuclides)
	$A < 100$ (160)	$100 \leq A < 200$ (301)	$A < 200$ (461)	$A \geq 200$ (90)	
StkI	808	422	584	716	609
StkII	795	424	579	720	607
LSD	895	502	673	342	630
MN	940	503	695	423	657
WK-D1S	978	695	805	972	834
WK-D1M	942	711	800	918	819

the considered set of 90 heavy and superheavy nuclei, the StkI and StkII *rms* values are 716 and 720 keV, which is larger than the *rms* deviations obtained for the same set of nuclei with the LSD and MN models, which are 342 and 423 keV, respectively. Possible reasons for the relative failure of the Stockholm models in the actinide and superheavy regions are the following. One of the reasons is a possible deficiency in the extrapolation of the Stockholm single-particle potential to these experimentally unknown regions and also the fact that the MN and LSD models use a richer deformation space. Another possible reason is the fact that the macroscopic part of the LSD model includes an explicit isospin dependence in the curvature term, which is absent in the Stockholm models by the reasons pointed out in Section 2.5.

5 Microscopic-macroscopic approach based on the Wigner-Kirkwood averaging method with the Gogny force

As we have discussed in the previous section, the use of the WK expansion to compute the shell correction allows one to obtain ground-state masses along the whole periodic table with a quality similar to that found for the same set of nuclei using the well-established Mic-Mac models such as the FRDM of Möller-Nix [40] or the Lublin-Strasbourg Drop [41], which use the Strutinsky averaging method to evaluate the shell correction. Following Ref.[42], we explore the interesting possibility of employing self-consistent single-particle potentials computed with effective nuclear interactions to calculate the shell corrections using the WK method. This idea reflects the imaginative and insightful nature of Peter Schuck, who invented it as an approach that would provide a link between the well-known mean-field approximation with effective forces and the Mic-Mac models. To this end, instead of the fully quantal mean-field potential obtained from the Hartree-Fock-Bogoliubov (HFB) scheme, we use, in the spirit of the so-called expectation value method [20,43], the semi-classical single-particle potentials developed in Ref. [44]. These potentials have been calculated in the Extended Thomas-Fermi (ETF) approximation (see [44] for further details). The ETF approach has been widely used together

with Skyrme forces for describing binding energies of finite nuclei at zero and finite temperature [20] as well as in the RMF framework [45,46]. The ETF approach has also been generalized to the case of non-local single-particle Hamiltonians [47] and, therefore, can be applied to the case of effective finite range forces, like the Gogny interaction [47–49].

5.1 Fitting procedure

In this Section we use the Gogny mean-field obtained with a Gogny force as external single-particle potential in order to compute the corresponding shell corrections and then to fit the macroscopic part of the energy by minimization of the residues of the theoretical minus experimental binding energies. As we have explained in Ref.[42], we proceed as follows in the particular cases of the D1S and D1M interactions. First, using the deformation properties for each nucleus obtained in the Mic-Mac WK calculation with the Stockholm-I single-particle potential we determine the parameters entering in the macroscopic energy Eq.(11), which in turn is used to determine the new deformation properties of the microscopic part by minimizing a second time the energy residues. However, with this protocol we find that the isotopes $^{182,184,186}\text{Pb}$ show a well-deformed structure in the ground state instead of being spherical as semi-magic nuclei of a robust proton shell closure $Z = 82$. As discussed with more detail in [42], it is found that this deficiency can be solved by considering the deformation properties not only of the macroscopic surface term (as in the case of the fit with the potential Stockholm-I [2]) but also of the curvature term.

The liquid drop parameters in Eq. (11) for the Gogny-based WK Mic-Mac model with the D1S as well as D1M forces fitted to the experimental energies [50] (without the electronic binding energy, which has been subtracted from the energies reported in [50]) of 551 even-even spherical and deformed nuclei are reported in Table 3. The complete list of energies of these 551 nuclei can be found in the supplemental material of Ref.[42]. The *rms* deviation of the energies from experiment is of 834 keV (819 keV) for Gogny D1S (D1M) based WK Mic-Mac model, as reported in the bottom row of Table 3. It has been explicitly verified that when the macroscopic part of our model is

fitted to Gogny-D1S HFB (Gogny D1M-HFB) energies, the corresponding HFB energies are reproduced very well (see Ref. [42] for further details). In Ref.[42] we have shown that the Gogny-D1S WK Mic-Mac model, whose macroscopic part is fitted to the HFB binding energies of 551 spherical and deformed even-even nuclei [51], is able to reproduce fairly well these quantal values with a similar *rms* deviation for the binding energies as the one provided by the full quantal HFB calculation [51]. This fact points out that the Mic-Mac approach used together with the underlying Gogny forces captures the essential physics of the full HFB calculation.

Table 3. Liquid drop parameters in Eqs. (11) and (12).

Parameter	D1S	D1M
a_v (MeV)	-15.903	-15.744
k_v	-1.855	-1.842
a_s (MeV)	20.265	19.171
k_s	-2.102	-2.072
a_{cur} (MeV)	-3.777	-2.498
r_0 (fm)	1.192	1.209
C_4 (MeV)	1.321	1.025
w_1 (MeV)	-1.528	-1.167
w_2	7.856	7.283
η	0.67	0.62
<i>rms</i> dev. (MeV)	0.834	0.819

5.2 Mic-Mac versus HFB calculations

In the right panels of Figure 3 we display the nuclear chart computed with the Mic-Mac WK model using the D1S (upper) and D1M (lower) mean-field potentials, respectively. For useful comparisons, we also show in the left panels of the same Figure the nuclear charts at full HFB level obtained with the D1S (upper) and D1M (lower) Gogny interactions. We see from the top left panel of Figure 3 that the HFB energies reproduces quite precisely the experimental values around magic proton and neutron numbers, as a consequence of the fitting procedure of the Gogny forces. However, the inter-shell region between magic numbers is not so well predicted with residues that in many cases are larger than +2 MeV. This fact is specially dramatic near the neutron-drip lines for heavy nuclei, in particular for the D1S force, where the well-known energy drift exhibited by this force [52] can be clearly appreciated. Also residues with a negative value smaller than -2 MeV can be seen around the proton drip line. The nuclear chart computed with the Gogny-D1S WK Mic-Mac model with the macroscopic part fitted to experimental masses shows a completely different pattern. We can see that it is much more similar to the one predicted by the WK Mic-Mac model using the phenomenological Stockholm potential by comparing the right upper panel of Fig.3 with the upper panels of Fig.2. This result points out that the WK Mic-Mac models with the macroscopic

part fitted to the experimental data are to some extent independent of the external potential used to determine the microscopic part. The underlying reason for that is the fact that the relatively small differences in the microscopic energies computed with different external potentials can be easily absorbed by the large macroscopic part through a variation of the liquid drop parameters. In this respect, it is expected that the energies predicted by the Gogny-based model starting from a different Gogny interaction, D1M [13] for example, will predict on average similar energies if the parameters of the macroscopic part are fitted to the experimental data, the differences with the results obtained using the D1S force, being relatively marginal. This is confirmed by the results shown in the lower right panel of Fig. 3 that correspond to the Gogny WK Mic-Mac calculation based on the D1M interaction instead of D1S.

As can be seen from the comparison between the left and right upper panels of Figure 3, the Mic-Mac model based on the Gogny D1S force with the macroscopic part fitted to the experimental masses, displayed in the right panel, also removes the drift in the HFB energies along isotopic chains shown in the left panel. As a consequence, it is expected that the Gogny WK Mic-Mac model can reproduce the experimental energies in heavy neutron-rich nuclei better than the pure HFB calculations using in both cases the same Gogny interaction. To analyze more in detail the differences between the full HFB and the Mic-Mac ground-state energies, we report in Table 4 the energies along the Pb isotopic chain computed at the HFB level [53] with the D1S and D1M forces and with our Gogny-D1S and Gogny-D1M WK Mic-Mac models, where the macroscopic part has been fitted to experimental masses. From this Table it is seen that along this isotopic chain the HFB energies exhibit a systematic behaviour with respect to the Mic-Mac Gogny results. In particular, we see that far from the shell closure at $N=126$, the Mic-Mac results agree nicely with the experimental values, while the HFB predictions show discrepancies with the experiment, which are more relevant in the case of the D1M force for the neutron-deficient Pb isotopes. However, near the shell closure, the HFB results computed with both, D1S and D1M forces, reproduce the experimental values fairly well, whereas, in turn, for these isotopes the Mic-Mac predictions slightly deteriorate.

A more quantitative information about the goodness of the Gogny WK models considered in this work is provided by the energy *rms* deviations with respect to experiment, which are reported in Table 2 in the entries labeled as WK-D1S and WK-D1M. For the set of considered nuclei, the *rms* deviations predicted by our WK Gogny model with the macroscopic part of the energy fitted to experimental masses is 834 keV for D1S and 819 keV for D1M. These deviations are a little larger than the ones obtained with the Mic-Mac WK model with the phenomenological StkI (609 keV) and StkII (607 keV) potentials, which in turn are quite similar to the ones predicted by the FRDM and LSD Mic-Mac models, as we have mentioned before. From the comparison of the upper panels of Figure 2 and right

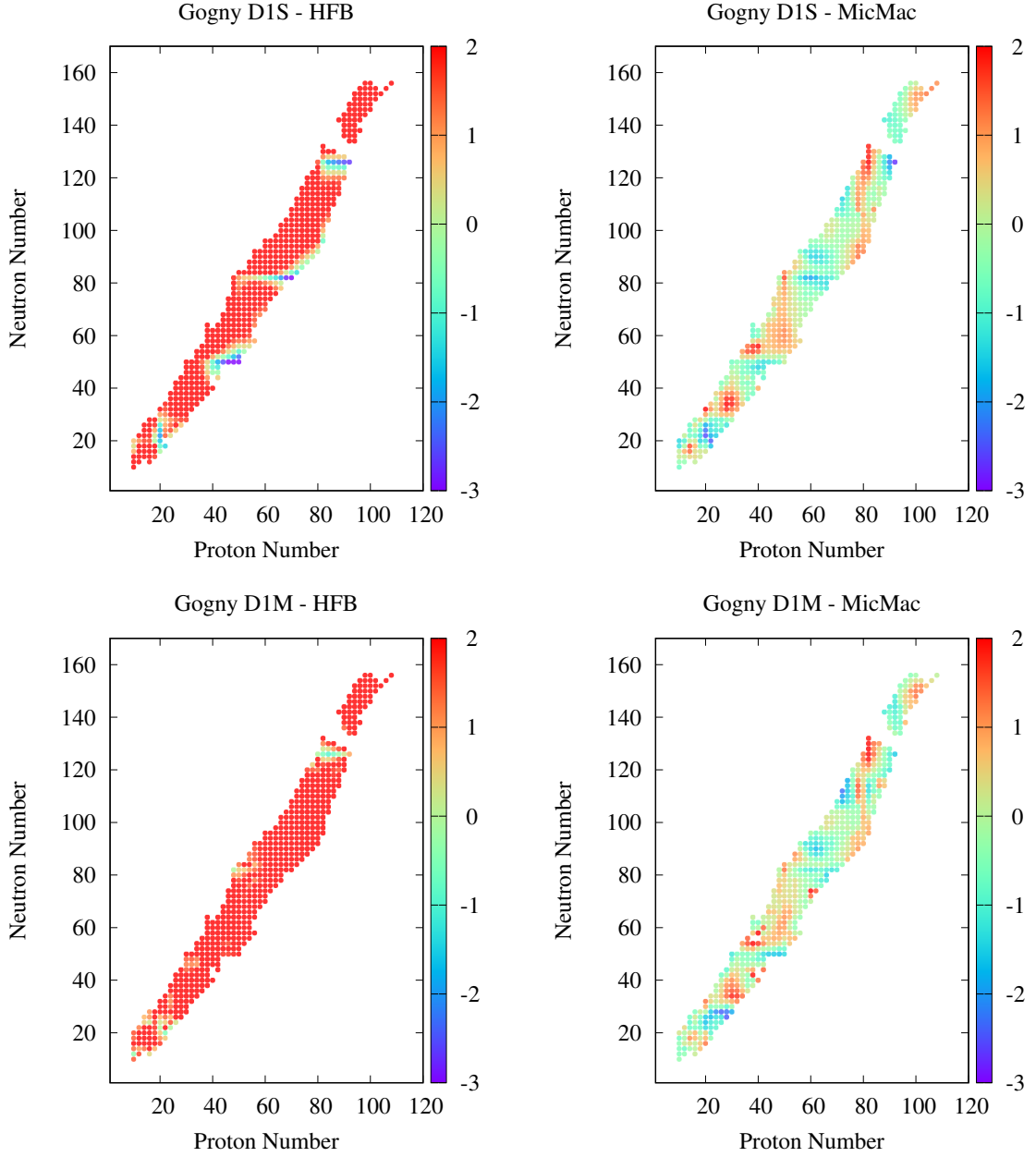


Fig. 3. Nuclear chart of theoretical minus experimental energies along the periodic table from Gogny HFB calculations with the D1S (upper left) and D1M (lower left) interactions as well as the results obtained with the Gogny+Mic-Mac method with D1S (upper right) and D1M (lower right).

panels of Figure 3, we can see that the prediction of the WK model based on the Stockholm potentials gives better description of the experimental energies in the range between $A \sim 100$ and $A \sim 200$ than the WK Gogny-based calculations.

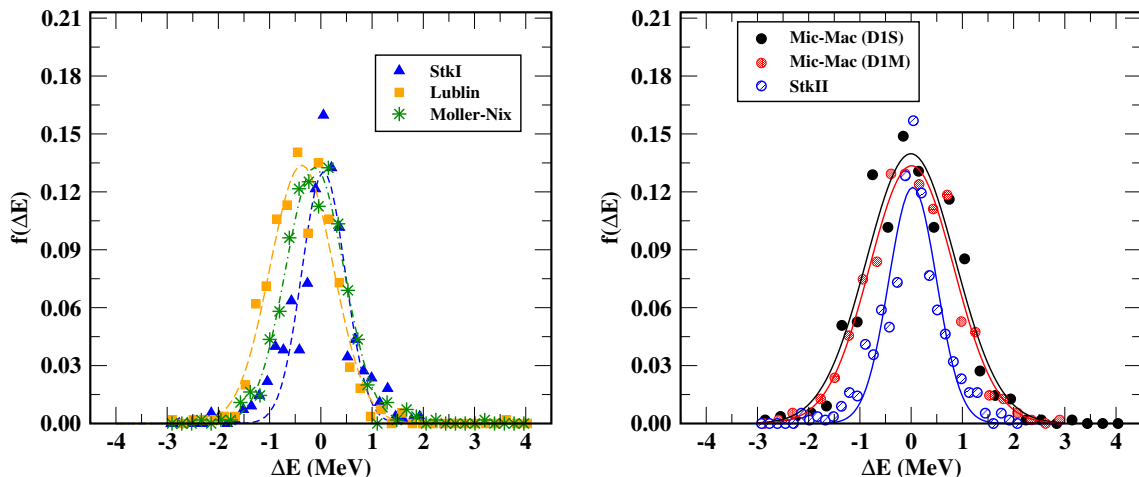
In spite of the fact that the global quality of the WK Gogny-based model is somewhat worse for describing ground-state energies as compared with the predictions of the other Mic-Mac models considered in this work (see Table 2), it is accurate enough to do predictions in good agreement with the experimental data.

6 Further investigations

Now we want to perform additional comparisons among the results obtained with our WK Mic-Mac models, both using the phenomenological Stockholm potentials and the mean-fields provided by the Gogny forces, and the predictions of the very well-known FRDM of Möller and Nix [40] and the LSD model of Pomorski and Dudek [41]. To this end we analyze the residues corresponding to 551 spherical and deformed nuclei with well-determined masses according to the Audi 2012 evaluation [50], which are displayed in Fig. 2 and the right panels of Fig. 3.

Table 4. Energies (in MeV) for Pb isotopes from the Gogny-D1S WK Mic-Mac model. The HFB D1S energies [53] and the experimental values [50] are also quoted for comparison. Notice that the contribution to the experimental energies from electronic binding has been removed here.

A	WK-D1S	HFB-D1S [53]	WK-D1M	HFB-D1M [53]	Expt.
178	-1367.60	-1369.13	-1367.50	-1361.81	-1368.40
180	-1389.28	-1389.94	-1389.24	-1383.13	-1390.05
182	-1410.37	-1410.26	-1410.43	-1403.95	-1411.08
184	-1430.90	-1430.09	-1431.08	-1424.28	-1431.45
186	-1450.88	-1449.44	-1451.20	-1444.14	-1451.23
188	-1470.31	-1468.37	-1470.80	-1463.56	-1470.50
190	-1489.26	-1486.88	-1489.93	-1482.56	-1489.25
192	-1507.70	-1505.02	-1508.56	-1501.17	-1507.54
194	-1525.58	-1522.79	-1526.66	-1519.42	-1525.32
196	-1542.83	-1540.20	-1543.99	-1537.30	-1542.62
198	-1559.33	-1557.26	-1560.30	-1554.83	-1559.45
200	-1575.19	-1573.96	-1575.87	-1571.99	-1575.79
202	-1590.56	-1590.28	-1590.98	-1588.79	-1591.63
204	-1605.48	-1606.21	-1605.66	-1605.19	-1606.94
206	-1619.91	-1621.66	-1619.85	-1621.14	-1621.76
208	-1633.29	-1636.44	-1633.06	-1636.46	-1635.86
210	-1643.09	-1643.79	-1642.93	-1644.74	-1644.98
212	-1652.12	-1650.81	-1652.03	-1652.70	-1653.95
214	-1660.87	-1657.49	-1660.84	-1660.40	-1662.72

**Fig. 4.** Binned data and the corresponding Gaussian fits for the different Mic-Mac models considered in the present study (see text for more detail).

From these Figures we can see that, globally, all the considered Mic-Mac models are quite equivalent for describing ground-state energies with residues that are not larger than ± 2 MeV along the whole periodic table. All these models show, roughly, similar trends, with the largest residues corresponding to magic numbers. Another common property of these residues is the fact that they are relatively larger for low mass than for heavy mass nuclei. The fact that all the models considered in this work behave more or less in a similar way requires a more detailed analysis. In order to do so and following Ref. [42], we have binned the residues $\Delta E = E_{cal.} - E_{expt.}$, i.e. the difference between the calculated and experimental energies, in a suitable way to get the normalized frequency distribution. The bin size was chosen carefully through the well-known

Freedman-Diaconis procedure [54,55]. In this analysis we use the results provided by the WK StkI and II, Gogny WK D1S, FRDM and LSD models.

The binned data for different Mic-Mac models plotted along with the corresponding fitted Gaussian profiles are displayed in the left (StkI, LSD and FRDM) and right (Gogny WK D1S, Gogny WK D1M and StkII) panels of Figure 4. We can see that all the six sets of data yield almost Gaussian profiles, with correlation coefficients greater than 0.95 in all the six cases. All the distributions have a central peak of height ~ 0.13 at $\Delta E \sim 0$, indicating that about 13% of the data is described with deviation of ~ 0 with respect to the experimental data. Apart from the different standard deviations in all the six models, the profiles of the residues were found to be very similar,

supporting the previous observation that all the six mass models are more or less equivalent, globally speaking. A more detailed inspection of the two panels of Figure 4 shows that binned data corresponding to our WK models are well centered around $\Delta E \sim 0$, while LSD and FRDM show a small shift towards negative ΔE values, which is more important for the LSD data. This fact indicates that on average our WK results are well scattered around the experimental energies while LSD and FRDM show a slight tendency of overbinding, at least for the considered set of nuclei. The widths of the Gaussian fits suggest that, for the considered set of nuclei, the quality of the WK results using the phenomenological Stockholm potential is somewhat better than the quality of the predictions of the FRDM and LSD calculations. From the right panel of this Figure it is also clear that the width of the Gaussian associated to the WK Gogny-based potential calculation is larger than the other widths displayed in the Figure, pointing out that the energy description for the set of considered nuclei provided by the WK Gogny-based Mic-Mac model is a fringe worse than the one obtained using the other models considered in this analysis.

7 Summary and conclusions

In this paper we collect some relevant results obtained with a Microscopic-Macroscopic model using the Wigner-Kirkwood expansion for evaluating the shell corrections instead of the Strutinsky averaging method, used in many mass models of this type, as for example the Finite Range Droplet Model of Möller and Nix or the Lublin Strasbourg Drop of Dudek and Pomorski. The use of the Wigner-Kirkwood approach instead of the Strutinsky average to compute the microscopic contribution to the energy avoids the problems of dealing with the continuum, on the one hand, and with the plateau condition, which is not always easy to establish [24]. Our model was developed together with Peter Schuck and the main findings of this investigation were reported in Refs. [1, 2, 44, 42].

In this work we have slightly modified the phenomenological single-particle potential used to get the microscopic energy by using the Coulomb potential obtained with a smooth proton distribution fitted to reproduce the experimental charge radii instead of a hard-sphere Coulomb potential used in our previous works Ref. [1, 2]. A detailed analysis performed with 551 spherical and deformed even-even nuclei in different mass regions reveals that the quality of these Wigner-Kirkwood Microscopic-Macroscopic models using the old, Stockholm-I, and the new, Stockholm-II, phenomenological potentials is as good as the quality provided by well established Mic-Mac models as the Finite Range Droplet Model or the Lublin-Strasbourg Drop.

In a second part of the paper we have combined the Wigner-Kirkwood Microscopic-Macroscopic approach with the mean field provided by the Gogny interaction instead of using the phenomenological Stockholm potential. The Gogny mean field is obtained via the semiclassical Extended Thomas - Fermi method, which includes \hbar^2 - corrections, with the Gogny D1S and D1M forces. In this

Microscopic-Macroscopic model the microscopic part is computed with the Wigner-Kirkwood method using the these Gogny D1S and D1M mean fields. The macroscopic part is fitted to the experimental binding energies of 551 spherical and deformed even - even nuclei, which is the database of our calculations. We find that the *rms* deviations of the binding energies in these calculations are 834 and 819 keV using the D1S and the D1M forces, respectively, which is slightly worse than the *rms* deviations obtained using the Stockholm potentials. The Microscopic-Macroscopic Wigner-Kirkwood models based on the Gogny forces calculations perform better in regions away of shell closures compared with the full HFB Gogny results, which are found to be better near shells corresponding to magic numbers.

A first conclusion of this work is that Wigner-Kirkwood based Microscopic-Macroscopic approximation is an interesting variant compared to the traditional Strutinsky average method. So far the former has produced results which are globally of similar quality to the other Mic-Mac approaches. At a finer level, one sometimes sees differences at proton and neutron numbers near the drip lines. A second relevant conclusion is that effective interactions, like Skyrme or Gogny forces, which depend on about ten adjustable parameters, are not able to yield optimal values of the macroscopic energy and, at the same time, an accurate description of the shell corrections. In contrast, a direct fit of the macroscopic part, via the liquid drop model, can optimize the smoothly varying macroscopic part of the binding energy, bringing it very close to its exact value.

In this work we have restricted our Microscopic - Macroscopic model with shell corrections computed with the Wigner-Kirkwood \hbar -expansion to discuss basically ground-state energies. The applications of the method to physical situations involving very large deformations, such as nuclear fission, requires to modify the distance function used in the calculations reported here. Work in this regard is undertaken.

Acknowledgments M. C. and X. V. acknowledge partial support from Grants No. PID2020-118758GB-I00 and No. CEX2019-000918-M (through the “Unit of Excellence María de Maeztu 2020-2023” award to ICCUB) from the Spanish MCIN/AEI/10.13039/501100011033.

References

1. A. Bhagwat, X. Viñas, M. Centelles, P. Schuck and R. Wyss, *Phys. Rev. C* **81**, 044321 (2010).
2. A. Bhagwat, X. Viñas, M. Centelles, P. Schuck and R. Wyss, *Phys. Rev. C* **86**, 044316 (2012).
3. H. L. Crawford *et al.*, *Phys. Rev. Lett.* **129**, 212501 (2022).
4. D. Vautherin and D. M. Brink, *Phys. Rev. C* **5**, 626 (1972).
5. Li Guo-Qiang, *J. Phys. G: Nucl. Part. Phys.* **17**, 1 (1991).
6. E. Chabanat, P. Bonche, P. Haensel, J. Meyer and R. Schaeffer, *Nucl. Phys. A* **635**, 231 (1998).
7. J. R. Stone and P.-G. Reinhard, *Prog. Part. Nucl. Phys.* **58**, 587 (2007).
8. S. Goriely, N. Chamel and J. M. Pearson, *Phys. Rev. Lett.* **102**, 152503 (2009).

9. S. Goriely, N. Chamel and J. M. Pearson, Phys. Rev. C **88**, 024308 (2013).
10. J. Dechargé and D. Gogny, Phys. Rev. C **21**, 1568 (1980).
11. J. F. Berger, M. Girod and D. Gogny, Comp. Phys. Commun. **63**, 365 (1991).
12. F. Chappert, M. Girod and S. Hilaire, Phys. Lett. B **668**, 420 (2008).
13. S. Goriely, S. Hilaire, M. Girod and S. Péru, Phys. Rev. Lett. **102**, 242501 (2009).
14. D. Vretenar, A. V. Afanasjev, G. A. Lalazissis and P. Ring, Phys. Rep. **409**, 101 (2005).
15. V. M. Strutinsky, Nucl. Phys. **95**, 420 (1969); **122**, 1 (1968).
16. P. Ring and P. Schuck, *The Nuclear Many-Body Problem* (Springer-Verlag, Berlin) (1980).
17. H. Krivine, M. Casas and J. Martorell, Ann. Phys. (NY) **200**, 304 (1990).
18. P. Schuck and X. Viñas, Phys. Lett. B **302**, 1 (1993).
19. M. Centelles, X. Viñas, M. Durand, P. Schuck and D. Von-Eiff, Ann. Phys. (NY) **266**, 207 (1998).
20. M. Brack, C. Guet and H.-B. Håkansson, Phys. Rep. **123**, 275 (1985).
21. H. P. Hohenberg and W. Kohn, Phys. Rev. **136**, B864 (1964).
22. Y. H. Chu, B. K. Jennings and M. Brack, Phys. Lett. B **68**, 407 (1977).
23. C. Mondal, X. Viñas, M. Centelles and J. N. De, Phys. Rev. C **102**, 015802 (2020).
24. B. Mohammed-Azizi and D. E. Medjadi, Phys. Rev. C **74**, 054302 (2006).
25. G. G. Bunatian, V. M. Kolomietz and V. M. Strutinsky, Nucl. Phys. A **188**, 225 (1972).
26. E. Wigner, Phys. Rev. **40**, 749 (1932).
27. J. G. Kirkwood, Phys. Rev. **44**, 33 (1933).
28. B. K. Jennings, R. K. Bhaduri and M. Brack, Nucl. Phys. A **253**, 29 (1975).
29. M. Brack and R. K. Bhaduri, *Semi-classical Physics* (Addison - Wesley Publishing Co.) (1997).
30. M. Centelles *et al.* Phys. Rev. C **74**, 034332 (2006) and references cited therein.
31. M. Centelles, P. Schuck and X. Viñas, Ann. Phys. **322**, 363 (2007).
32. A. Bhagwat, R. Wyss, X. Viñas and P. Schuck, Int. J. Mod. Phys. E **19**, 747 (2010).
33. S. Cwiok, J. Dudek, W. Nazarewicz, J. Skalski, and T.R. Werner, Comp. Phys. Comm. **46**, 379 (1987).
34. W. Nazarewicz *et al.* Nuc. Phys. A **435**, 397 (1985).
35. I. Angeli, At. Data Nucl. Data Tables **87**, 185 (2004).
36. W. Satula and R. Wyss, Rep. Prog. Phys. **68**, 131 (2005) and references therein.
37. H. J. Lipkin, Ann. Phys. (N.Y.) **9**, 272 (1960).
38. Y. Nogami, Phys. Rev. **134**, B313 (1964).
39. H. C. Pradhan, Y. Nogami and J. Law, Nucl. Phys. A **201**, 357 (1973).
40. P. Möller, J. R. Nix and K. -L. Kratz, Atom. Data Nucl. Data Tables **66**, 131 (1997).
41. K. Pomorski and J. Dudek, Phys. Rev. C **67**, 044316 (2003).
42. A. Bhagwat, M. Centelles, X. Viñas and P. Schuck, Phys. Rev. C **103**, 024321 (2021).
43. O. Bohigas, X. Campi, H. Krivine and J. Treiner, Phys. Lett. B **64**, 381 (1976).
44. A. Bhagwat, M. Centelles, X. Viñas and P. Schuck, Phys. Rev. C **103**, 024320 (2021).
45. M. Centelles, X. Viñas, M. Barranco and P. Schuck, Nucl. Phys. A **519**, 73 (1990).
46. M. Centelles, X. Viñas, M. Barranco and P. Schuck, Ann. Phys. (NY) **221**, 165 (1993).
47. V. B. Soubbotin and X. Viñas, Nucl. Phys. A **665**, 291 (2000).
48. K. A. Gridnev, V. B. Soubbotin, X. Viñas and M. Centelles, *Quantum Theory in honour of Vladimir A. Fock*, Y. Novozhilov and V. Novozhilov (Eds.) Publishing Group of St.Petersburg University 1998, p.118; arXiv 1704.03858.
49. V. B. Soubbotin, V. I. Tselyaev and X. Viñas, Phys. Rev. C **67**, 014324 (2003).
50. G. Audi, M. Wang, A. H. Wapstra, F. G. Kondev, M. MacCormick, X. Xu and B. Pfeiffer, Chin. Phys. C **36**, 1287 (2012).
51. CEA web page www-phynu.cea.fr.
52. N. Pillet and S. Hilaire, Eur. Phys. J. A **53**, 193 (2017).
53. L. M. Robledo, HFBaxial computer code (2002).
54. D. Freedman and P. Diaconis, Z. Wahrscheinlichkeitstheorie verw. Gebiete **57**, 453 (1981).
55. A. J. Izenman, J. Am. Stat. Assoc. **86**, 205 (1991).